Soft Matter

PAPER

View Article Online
View Journal | View Issue

Cite this: *Soft Matter*, 2020, **16**, 9899

Dynamics of progressive pore clogging by colloidal aggregates†

N. Delouche,[a] A. B. Schofield [b] and H. Tabuteau *[a]

Received 4th August 2020,
Accepted 28th September 2020

DOI: 10.1039/d0sm01403f

rsc.li/soft-matter-journal

The flow of a suspension through a bottleneck often leads to its obstruction. Such a continuous flow to clogging transition has been well characterized when the constriction width to particle size ratio, W/D, is smaller than 3–4. In such cases, the constriction is either blocked by a single particle that is larger than the constriction width ($W/D < 1$), or there is an arch formed by several particles that try to enter it together ($2 < W/D < 4$). For larger W/D ratios, $4 < W/D < 10$, the blockage of the constriction is presumed to be due to the successive accumulations of particles. Such a clogging mechanism may also apply to wider pores. The dynamics of this progressive obstruction remains largely unexplored since it is difficult to see through the forming clog and we still do not know how particles accumulate inside the constriction. In this paper, we use particle tracking and image analysis to study the clogging of a constriction/pore by stable colloidal particles. These techniques allow us to determine the shape and the size of all the objects, be they single particles or aggregates, captured inside the pore. We show that even with the rather monodisperse colloidal suspension we used individual particles cannot clog a pore alone. These individual particles can only partially cover the pore surface whilst it is the very small fraction of aggregates present in the suspension that can pile up and clog the pore. We analyzed the dynamics of aggregate motion up to the point of capture within the pore, which helps us to elucidate why the probability of aggregate capture inside the pore is high.

Introduction

The flow of colloidal suspensions in confined environments often leads to partial or complete clogging in various contexts including natural flows inside soils and rocks,[1] filtration through a membrane,[2] during chemical synthesis[3] or transport in micro-engineered channels,[4] porous networks[5] and reactors.[6] Three main mechanisms have been identified to explain pore clogging by spherical particles, which depend on the width to particle size ratio, W/D.[4] Firstly, there is clogging by sieving for particles bigger than the mean pore/channel size[7,8] or for pores whose dimensions are 2–3 diameters of the particles, $W/D < 2$–3, hydrodynamic bridging occurs when several particles try to enter the pore together.[9–11] Finally for even larger pores the clogging process is progressive and there is an accumulation of particles until pore blocking happens.[12–16]

Microfluidic experiments have largely helped to quantify and better understand the way clogs are formed. This technology, that emerged twenty years ago, gives access to various geometric features in 2D[17] and more recently in 3D[18] such as those encountered in membranes used in the filtration processes inside industrial equipment. The transparent model filters made by this technique enable us to follow and track particles up to the point of their capture by the surface of the pores.[14,19,20] Most of the previous clogging studies have focused on the impact of the geometry of the pore,[13,14,21–23] focusing particularly on the influence of the confinement,[12–14] as discussed above. Others have looked at the influence of the particles' properties like the interparticle interactions or the interactions between the particle-and pore surface[12,13,21,24–26] and the effect of the polydispersity of the suspension.[7,8,27] More recently, studies on the clogging of model filters have been performed with deformable particles like microgels.[28–30] Finally, microfluidics has been used to determine under which conditions a pore blocked by colloidal particles can be de-clogged by reversing the flow.[31] Among this growing set of publications most of them provide images of the pore either partially or completely clogged,[21,28,32–35] but only few have gone further and considered the behavior of the particle inside a clog or in a deposit.[14,15,29] The dynamics of particle deposition have been monitored only in very confined situations for both non Brownian[36,37] and colloidal particles.[14] No such dynamics have been provided at the particle level for progressive fouling since it requires challenging imaging conditions to see through the

[a] Univ Rennes, CNRS, IPR (Institut de Physique de Rennes)-UMR 6251, F-35000 Rennes, France. E-mail: herve.tabuteau@univ-rennes1.fr
[b] School of Physics and Astronomy, The University of Edinburgh, The James ClerkMaxwell Building, The King's Buildings, Mayfield Road, Edinburgh, UK

† Electronic supplementary information (ESI) available. See DOI: 10.1039/d0sm01403f

forming clog.[15] In such mild confinement, for $4 < W/D < 10$, with W and D respectively the pore width and the particle diameter, particles partly cover the pore surface and at some point, they are supposed to start accumulating on top of this first layer until the pore is finally blocked. However, several works have pointed out that in such confinement the fouling process may be not due to the progressive accumulation of monodisperse particles. Gerber *et al.*,[38] show that particles can form only a monolayer on glass beads in a 3D packed bed when the ionic strength is low compared to the critical coagulation concentration. Others experiments in transparent model filters have shown that frequently particles of different sizes are involved in the clogging process. Even though they worked with monodisperse suspensions, they found that a few particles in the suspension, larger than the mean size, are mainly responsible for pore blocking. Either their size is bigger than the pore size leading directly to pore blocking; the particle being arrested at the pore entrance, or smaller particles first deposit on the pore surface, forming a monolayer, and then a larger one blocks the remaining part of the pore cross section.[7,8,27] Such pore blocking is often seen when one uses natural and engineered suspensions that are composed of aggregates and are polydisperse in shape and size. For instance, injections of therapeutic proteins like monoclonal antibodies often contain aggregates so large that they lead to clogging of the needle or infusion catheters[39] and flocculated clay particles form large aggregates that are responsible of the clogging of membrane filters[40] and drippers in microirrigation.[41]

When there is a salt gradient and colloidal particles flowing through a porous network we also observe pore clogging as in a reverse osmosis membrane.[42] Microfluidics has also helped to better understand how aluminium salts used in antiperspirants gels lead to the aggregation of sweat proteins which block eccrine sweat pores.[43] Shin *et al.*, show that flows in porous media can induce strong diffusiophoretic focusing at fluid junctions where particles spontaneously accumulate until their concentration is high enough to cause a blockage.[44] This localized salt gradient can lead to irreversible blocking by particles two orders of magnitude smaller that the pore width.

Clogging issues are also often encountered when solid particles are formed under flow either by mixing different species[45] as for instance during the formation of kidney stones[46] or as a product of chemical reactions. During flow chemistry, the solid particles and aggregates produced are transported by the flow and deposited inside the processing equipment.[47,48] These aggregates grow continuously due to the constant supply of reactants and also help to capture other flowing aggregates or isolated particles.[3] The growth under different flow conditions leads to different shapes and morphologies of aggregates, which can also be fragmented by the flow.[49,50]

As far as we know nobody has determined the different features of the clogging dynamics at the pore scale by such particle aggregates even though they make up most of the natural and industrial colloidal suspensions. In this paper we describe clogging experiments with a dilute, stable against aggregation, mostly monodisperse colloidal suspension inside a microfluidics model porous medium over a wide range of applied pressures. During these experiments we systematically monitor the deposition history of colloidal particles within a pore and the mean size and shape of each deposited object. These observations allow us to show that there is a major influence from a minute quantity of aggregates present in our monodisperse suspension. There is no progressive accumulation of single particles alone leading to the pore clogging. These particles can only form a monolayer on top of the pore surface onto which a small number of aggregates deposit and eventually block the pore. The higher deposition rate of aggregates directly on the pore walls or on the colloidal monolayer deposit is due to their rotation around their center of mass that increases significantly their physical capture at a higher distance from the pore/deposit surface than is seen for single particles.

Materials and methods

Microfluidics filter and image analysis

We used standard methods of soft lithography and PDMS molding[51] to build our microfluidic device. We followed the same protocol used by Dersoir *et al.*,[15] to obtain a model filter completely made of PDMS in order to have the same colloidal interactions between the particles and the lateral and horizontal walls of the device. The device is 12 μm high and composed of two large channels on both sides of a model filter made of 26 identical and independent channels in parallel (Fig. 1a and b). Each channel is composed of two consecutive reservoirs connected to a pore, which corresponds to the narrowest part of the filter with a width W equal to 7 μm, which corresponds to a pore width-mean particle size ratio equal to 3.9 (Fig. 1c). When the pore is clogged, the two reservoirs are never completely filled by particles which avoids the premature clogging of the two

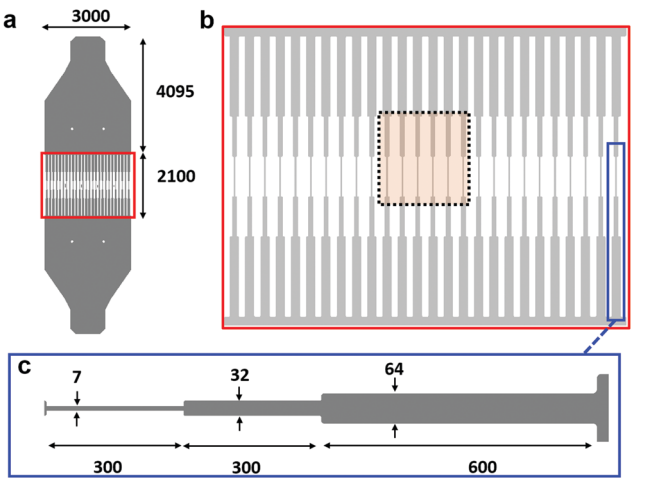

Fig. 1 (a) Model filter with inlet and outlet and the filtering zone in the middle, highlighted by the red rectangle (colour online). (b) Zoom of the filtering zone composed of 26 identical channels. The dotted rectangle corresponds to the zone which is imaged by the camera. (c) Details of the channel geometry with the thinnest part corresponding to the pore, on the left, and the two reservoirs on the right. All the dimensions are given in μm.

adjacent channels. During the experiments we image only the six channels in the middle of the filter (Fig. 1b, dotted rectangle), which allows us to use an acquisition frame rate high enough to perform particle tracking (PT) on all the particles that flow through both the pore and the reservoir just upstream. The experiment is stopped when these six channels are clogged. We image the transport of fluorescent particles with a SCMOS camera (Hamamatsu Orca Flash 4.0).

To flow the suspension, we used a precise microfluidics pressure control system (Elveflow OB1 Mk2 or Fluigent MSFC) to impose a constant pressure gradient between the pore inlet and the outlet. We work with a wide pressure range (0.5 mbar to 120 mbar) corresponding to a flow rate Q at the beginning of the experiment, between 0.008 and 0.9 μL min^{-1}. There is an increase of W is lower than 0.5 μm for the highest applied pressure. We measure this flow rate by weighing the mass of water flowing through the device for one hour with an analytical scale, with an accuracy of 0.2 mg, connected to the device outlet. Since we work with a pressure gradient the clogging of several pores does not significantly change the flow rate in the other pores. The Reynolds number is always smaller than 10^{-3} and the Péclet number is high and between 1.6×10^4 to 5.2×10^6. Under these conditions inertia and particle Brownian diffusion are negligible.

The particles with a diameter D = 1.8 μm were synthetized following the procedure detailed in Shen *et al.*[52] They are made of PMMA in which a NBD (7-nitrobenzo-2-oxa-1,3-diazole) dye is incorporated. These particles use a polymer brush coating, composed of polyvinylpyrrolidone chains that bear negatives charges, to stabilize themselves against aggregation. The resulting zeta-potential is equal to −70 mV. We used a mixture of water (33% by weight), urea (37%) and glycerol (30%) in order to obtain an isodense suspension to negate particle sedimentation over the course of the entire experiment.

Suspension characterization

Characterization of aggregates. The monodisperse suspensions are characterized by a size distribution with a peak around the mean diameter of the particles. However, like all monodisperse suspensions, we also find contaminants, mainly particle aggregates and to a lesser extent large particles. The aggregates are likely formed at the beginning of the particle synthesis when the semi-stable PMMA particles are rapidly growing and by random chance encounter other such particles.[53] This may lead to the formation of few stabilized aggregates. Those aggregates are composed of 1.8 μm particles which seems to be linked permanently to each other. Examples of such aggregates are shown in Fig. 2. We checked that the distributions of aggregate shape and size do not change when these aggregates flow through the different parts of the model filter where they experience various levels of shear. From this we conclude that the aggregates of our suspensions are stable against shear flow and their distribution does not evolve as they flow through the model filter. We also added various amount of salt and determined the aggregate size distribution and found no difference even for salt concentrations where the surface charge of the polymer brush is completely screened. This confirms that both particles and aggregates are stabilized by the polymer brush grafted on their surface. This means there is a steric stabilization of all the types of particles which prevent them from adhering to each other.

To characterize the size distribution of the different objects that compose the suspension we inject a suspension with a very low volume fraction of 5×10^{-4} into a rectangular channel (1 cm long, 0.5 mm wide and 20 μm high). During this experiment, we stop the injection for 6–7 s and image the particles in one part of the channel. Thereafter we flush the channel with a large pressure for 3–4 s, high enough to get new particles in the image. In this way, we obtain typical pictures with around 1200–1400 objects and after 7–8 h of experiment, we obtain a total amount of roughly 3.3×10^6 objects. In each image we start by detecting the particle position and determine whether it is in an aggregate or not. To locate and characterize fluorescent particles, the most commonly used method is Gaussian fitting. Due to the proximity of neighbouring particles within an aggregate there is an overlapping of their respective Gaussian fits, which makes it difficult to distinguish each particle (triplet in Fig. S1a, left, ESI†). In addition, when particles are well packed inside an aggregate the intensity distribution can be so smoothed that the algorithm eventually detects only one particle (quintuplet in Fig. S1b, left, ESI†). To overcome these difficulties, we use fast radial symmetry[54] which detects zones with a high radial symmetry from gradients in the images. Rather than looking at the contribution of the pixels around a central one, the FRS algorithm quantifies the contribution each pixel makes to the symmetry of pixels around it. Thanks to this method, we are able to determine the particle centre of overlapping particles inside the aggregates (Fig. 2). Secondly, we determine the centroid of the projected areas of the aggregates. The coupling of this second step with the FRS method gives us access to the number of particles within an aggregate and also the geometrical descriptors of the aggregates (Fig. S1 and S2, ESI†).

We use a particle tracking method at 100 frames per second to capture the aggregate dynamics under flow, with a flow rate of 0.05 μL min^{-1} and a low particle concentration of 5×10^{-3}. This method is able to discriminate adjacent flowing particles and also those which are deposited in the reservoir. Using the FRS method and the centroid detection, we get various useful features of the flowing aggregates (orientation, shape and number of particles inside an aggregate).

We systematically determine the type and size of the objects that flow through the microfluidic filter during the clogging experiments, with an acquisition frame rate sufficiently high, between 3 to 30 fps, to be able to monitor separately each object that deposits. The type of captured aggregate is determined manually and the capture probability is calculated from the number of flowing particles through the pore and the distribution obtained from the stop and go experiments.

Results and discussion

We have previously performed clogging experiments with 4 μm particles in two confined situations ($1.5 < H/D < 3$) where

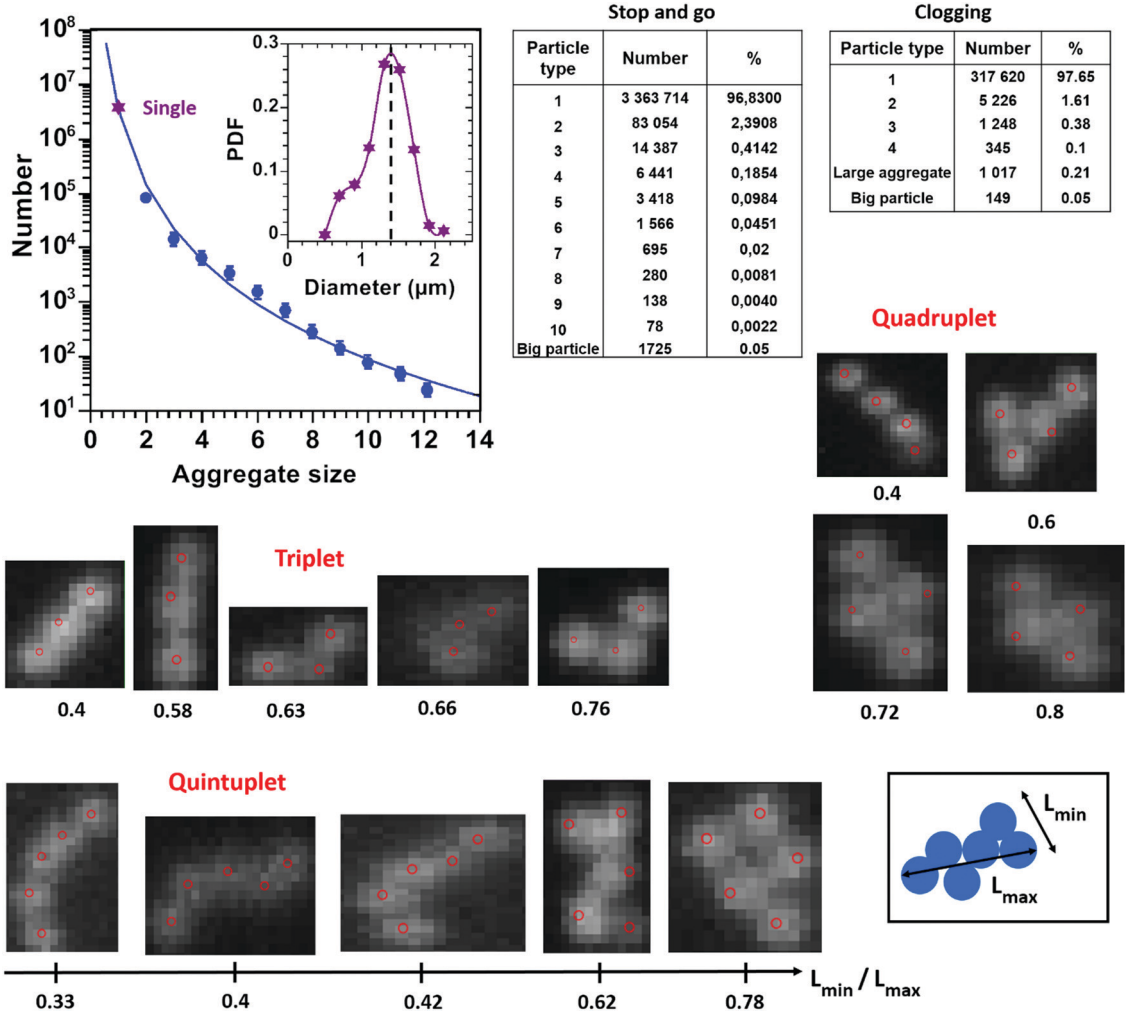

Particle type	Number	%
1	3 363 714	96,8300
2	83 054	2,3908
3	14 387	0,4142
4	6 441	0,1854
5	3 418	0,0984
6	1 566	0,0451
7	695	0,02
8	280	0,0081
9	138	0,0040
10	78	0,0022
Big particle	1725	0.05

Particle type	Number	%
1	317 620	97.65
2	5 226	1.61
3	1 248	0.38
4	345	0.1
Large aggregate	1 017	0.21
Big particle	149	0.05

Fig. 2 (top-left) Distribution of aggregate sizes inside the PMMA suspension. The size of aggregates corresponds to the number of particles within an aggregate. The continuous line is a power law fit of the data with power index of −4.4. (inset) Particle size distribution of the single particles determined from image analysis, which is centred on 1.4 μm. More accurate size measurements from MEB images lead to a greater mean particle size of 1.8 μm. (right) Proportion of the different types of particles that composed the PMMA suspension from the "stop and go" and the "pore clogging" experiments. (bottom) Examples of images of triplets, quadruplets and quintuplets with different shapes characterized by the ratio L_{min}/L_{max}, defined in the scheme in the bottom right corner.

particles captured by the pore walls lead directly to the clogging of the pore.[14,15] More precisely, there is no need to accumulate particle on each other to block the pore, *i.e.*, the formation of particle monolayers on the different pore surfaces lead to the pore blocking. Thanks to confocal microscopy we were able to monitor the clog formation at the particle scale by following the particle deposition individually. We show in both studies that self-filtration is the main mechanism of pore clogging since the confinement is rather high. After the deposition of a few particles inside the pore by direct interception by the pore walls, the following deposition events are due to hydrodynamic interactions between those immobile objects and those about to be captured. The influence of aggregates was rather limited since we observed very few aggregates larger than doublets being captured within the pores. Even though confocal imaging is a very powerful tool to get the structure of the clog it does not give access to the dynamics of particle deposition, which is the goal of the present work. Here, we perform clogging experiments in long pores but in a less confined configuration where we flow smaller, 1.8 μm PMMA particles through 8 μm wide and 12 μm high pores. In this case there must be particle accumulation over several layers in addition to the initial particle monolayer in contact with the pore walls to completely obstruct the pore. Rather than using confocal microscopy we use a SCMOS camera able to track particles when they flow through the pore which means that, in contrast to our previous studies,[14,15] we do not have access to the structure within the forming clog. Instead, we are able to determine the dynamics of the particles as they get captured, and also their size and shape, which allows us to determine the aggregate size distribution as the aggregates flow through the pore.

Major contribution of aggregates to pore clogging

We first count the number of particles deposited inside the pore for flow rates, Q, between 0.008 and 0.9 μL min^{-1}. The

clogging process is not due to the progressive deposition of single particles alone, as is presupposed,[12,13,25] even though the suspension is rather monodisperse with around 97% of the particles having the same size (Fig. 2, left table). Single particles are mainly captured on the pore walls by physical interception, but they are then unable to pile up on that initial monolayer to progressively clog the pore (Fig. 3a). It turns out that particle aggregates, which corresponds to 3% of the particle population, are mainly responsible of the pore clogging. Whatever the flow rate there are three to five aggregates, from doublets up to aggregates composed of 10–12 particles, that deposit inside the pore in each experiment (Fig. 3b–d). The capture of these aggregates also facilitates the deposition of isolated single particles as these capture events lead to the formation of a porous deposit through which fluid can still flow and individual particles that follow these fluid paths can get trapped.

Since we have enough aggregates, (Fig. 2, right table), we are able to determine their probability of capture, which is the ratio of the number of aggregates deposited over the total number that flow through the pore, for each aggregate type. Note that there are large variations of this probability from one experiment to another since the history of the clogging formation for a given pore, *i.e.*, the successive particle–aggregate deposition process, is unique. However, since we have performed an important number of trials clear trends emerge from the variation of the capture probability with Q (Fig. 4).

The capture of aggregates, irrespective of their size, is much higher than the deposition of single particles for the full range of Q. For $0.02 < Q < 0.24$ μL min^{-1} there is a sharp decrease in the capture probability corresponding to a lower particle deposition by physical interception by the pore walls,[14] for all particle types. From $Q > 0.2$–0.4 μL min^{-1} the capture probability does not change with Q for aggregates while there is a very slight decrease for single particles. In this flow regime the physical interception of particles by the pore walls is the smallest while capture by the deposit, *i.e.*, by particles already stuck in the pore, remains constant. It is worth noting that the capture probability increases rapidly with the number of particles within an aggregate, irrespective of the flow rate. This is intuitively related to the aggregate's dimensions, the bigger the aggregate the more they are confined and the closer to the pore walls they are, enhancing their capture. However it is not just a question of size since particles bigger than the mean size are also present in the suspension and these have a very limited contribution to the pore clogging even though they quite numerous (Fig. 2, left table). Indeed, big particles, with a diameter smaller than the width of the pore, can be easily wiped off the pore walls by the flow since they experience high shear variations. In the case of aggregates they can withstand higher shear stresses as their structures are more open, reducing the torque due to the shear, since the fluid can pass through them.[55] In addition, aggregates have multi-contact with either the pore wall and/or the deposit that increases significantly their stability against removal by the flow. This is particularly true for the aggregates formed from four or more particles for which we observe that their capture probability remains high and varies between 0.3 and 0.7 over the range of Q we used.

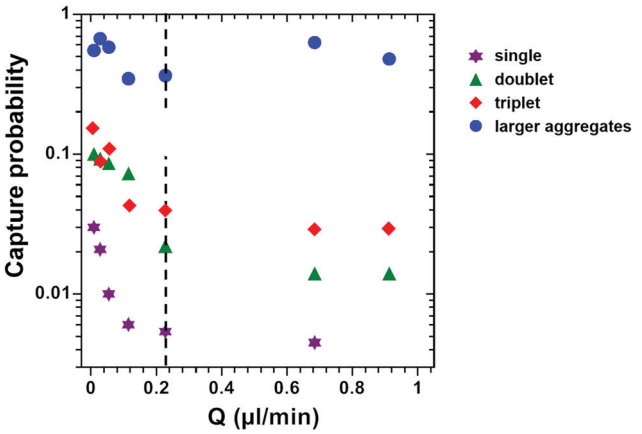

Fig. 4 Variation of the capture probability of single and aggregate particles with the flow rate Q. The dashed line corresponds to the limit between the two flow regimes.

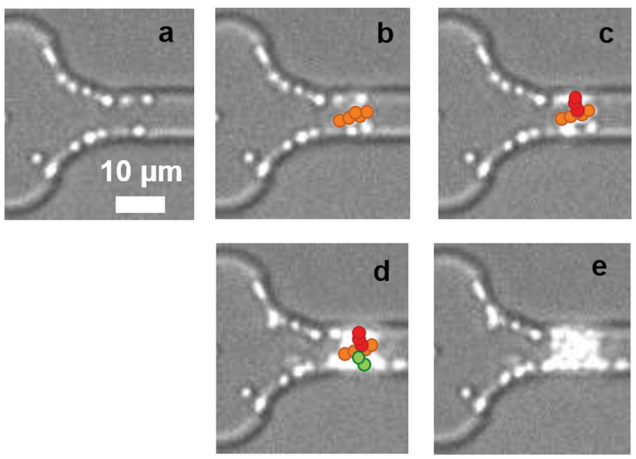

Fig. 3 Successive images for pore clogging by single particles alone (a) and aggregates, a quintuplet in (b), a triplet in (c) and a doublet in (d). The pore is completely obstructed by few additional single particles in each step. All the deposited aggregates were identified as they flowed through the reservoir zone prior their deposition. The position of these captured aggregates in the pore is approximate since this is a 2d view of the pore constructed to show that the aggregates were effectively immobilized in the forming clog. Note that individual particles are also captured by the deposited aggregates but we do not highlight their position in the clog so as not to overload the images.

To identify the underlying physical processes that are responsible for the capture of aggregates we look at their dynamics near the pore entrance, following their motion from the reservoir zone up to their capture by the pore walls or the deposit inside the pore. In this way we will be able to determine the features of the physical interception of aggregates. The interception of spherical particles by the pore walls is well known.[12,56] In our filter geometry spherical particles flow through the reservoir and follow a given straight streamline along its path. When the particle get closer to the pore entrance, the width of the channel is narrower leading to a compression of the streamlines, which allows the particle to

move from its original streamline to another that is closer to the surface of the pore wall. At some point the particle cannot avoid the pore surface, due to its finite size, and comes sufficiently close to the surface, below tens of nanometer from it, and falls in the attractive part of the interaction potential between the particle and the pore surface and thus becomes stuck.[12]

Whatever their size and shape aggregates rotate periodically during their transport through the microchannel (Fig. 5a–c and Fig. S3, ESI†), like a rod that exhibits Jeffery orbits in pure shear flow.[57,58] This means that even though the center of mass of an aggregate remains located on the same streamline in the reservoir, just upstream of the pore, their edges come periodically closer to the nearby pore walls. However, contrary to the simple case of rods, in our experiments there are large variations in the dynamics of the aggregate spinning process due to the flow conditions in high confinement and there are

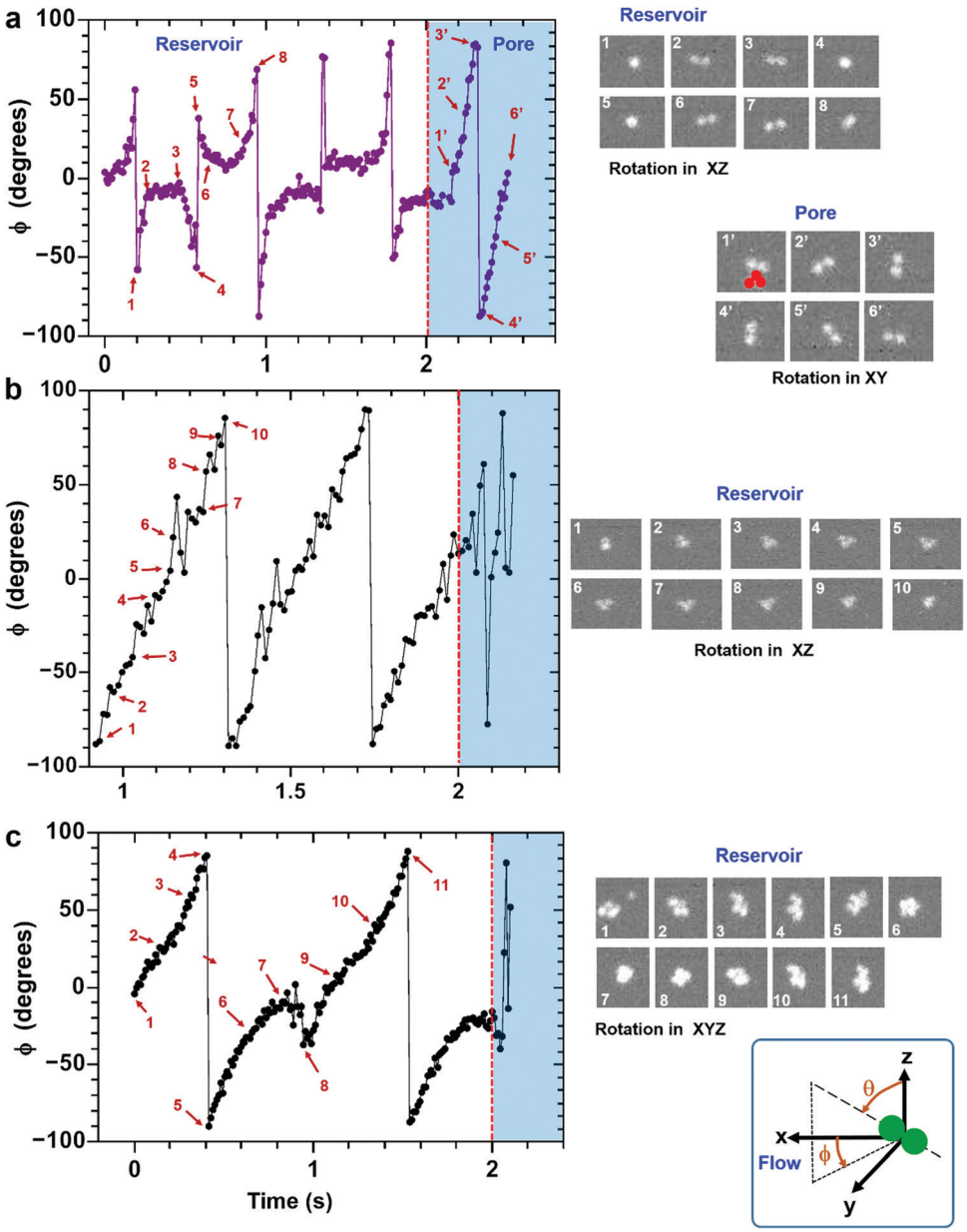

Fig. 5 (a) Variation of the orientation ϕ in the XY plane (see sketch on the bottom left corner), parallel to the top and bottom surfaces of the pore and corresponding to the observation plane of the microscope, for a doublet that flows consecutively in the reservoir and then in the pore. The numbers refer to the images on the left. The long axis of the doublet is in the z-direction at the beginning and the end of each period (images 1, 4, 5 and 8). Inside the pore the trajectory of the doublet is modified by the deposit (the red triplet is in contact with the pore wall) in image 1′. (b) Variation of the orientation for a flat triangular shaped triplet until it gets captured inside the pore. At the beginning of each period the triplet lies completely in the YZ plane, perpendicular to the flow direction (images 1 and 10), while at the middle of the period it lies in the XY plane, parallel to the top and bottom surface of the channel (image 5). (c) Variation of the orientation for a large aggregate with a complex shape and composed of at least of 6 particles. The dynamics of deposition inside the pore for the triplet (b) and the large aggregate (c) are shown in Fig. 6a and b, respectively.

especially important variations of the shear along the height of the channel. These lead to additional hydrodynamic interactions of the aggregates with the pore walls, modifying the spinning process especially at the transition between the reservoir and the pore. For instance, for the doublet in Fig. 6, upstream of the pore, it rotates along the flow direction in *XZ* plane, the plane perpendicular to the lateral walls of the pore, *i.e.*, it has a tumbling motion in the reservoir. We observe an important change in the doublet's rotation dynamics at the pore entrance (red dashed line in Fig. 5a). At this position the channel becomes more confined along the width (8 μm) than along the height (12 μm) leading first to an increase of the local fluid velocity and more importantly, to a modification of the orientation of the aggregate.

In less than 30 μm, corresponding to the distance over which the channel is progressively narrowed, the doublet rotates in all planes and then becomes stabilized when the pore section no longer changes, rotating only in the *XY* plane, parallel to the top and bottom walls as it travels along the pore (see also Fig. 6a for the case of a triplet that deposits and Fig. S3 for other examples, ESI†). This means that when the pore cross section becomes constant the doublet finds an equilibrium position relative to the pore surfaces and performs periodic rotations, while at the pore entrance the edges of the doublet can come closer to the lateral walls of the channel increasing its probability of being captured at this point. Such modifications of both the rotation planes and the trajectory also occur when aggregates encounter a particle/aggregate attached to the pore surface (Fig. 6c). We suggest that this rather fast modification of the aggregate orientation leads to their capture mainly near the pore entrance and no further than 30–40 μm inside the pore, as illustrated in Fig. 6a–c, where various aggregate types encounter new flow conditions as they either enter a pore or come across the surface of the deposit inside the pore. During that short moment one of their edges cannot avoid touching the pore walls (Fig. 6a and b). This is also true when aggregates come across particles/aggregates already deposited at the pore surface (Fig. 6c). An important observation, which confirms our hypothesis, is that almost no aggregate deposition occurs inside the pore far downstream of the entrance. Most of the time aggregates find a new equilibrium position around which they rotate without any possibility of touching the pore walls as they flow through the pore. However aggregates can still be stopped anywhere within the pore if they encounter other particles/aggregates or a channel defect; events which are rare in our set of experiments.

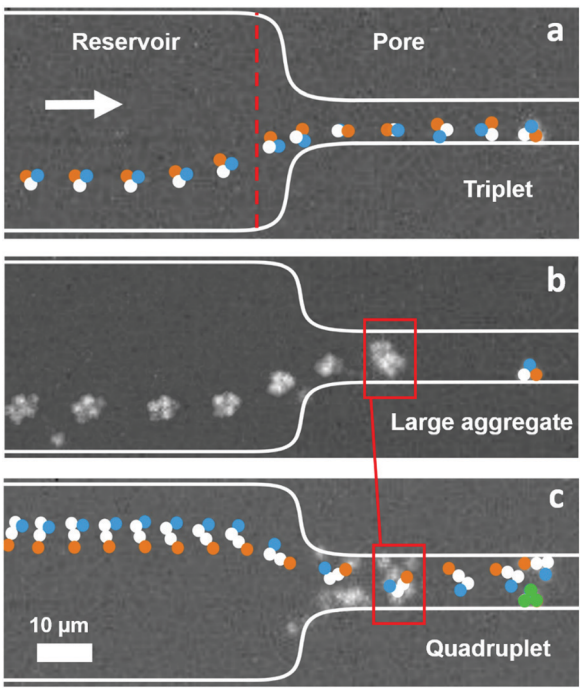

Fig. 6 Deposition dynamics of various aggregates inside the same pore for Q = 0.05 μL min^{-1}. The different colors in (a) and (c) help to see the abrupt variation of rotation of the aggregates as they enter the pore. The arrow points in the flow direction while the dashed line in (a) corresponds to the transition between the reservoir and the pore. The red squares in (b) and (c) outline the final position of the large aggregate deposited in (b), around which the quadruplet performs an abrupt rotation, while the green triplet corresponds to the first deposition event in this pore that takes place in (a).

As already mentioned above, similarly to spherical particles, aggregates have to flow near the lateral walls of the reservoir, upstream of the pore, to be captured by physical interception by the pore walls. Aggregates that are closer to the lateral walls of the reservoir zone have more chance of being captured further downstream at the pore entrance since they have to flow very close to the walls at that location (Fig. 6a, b and Fig. S2, ESI†). After the capture of several particles and aggregates inside the pore there is also physical interception of flowing aggregates but this time by these immobile particles that compose the deposit (Fig. 6c). In such a case, there is no dependence on the position in the reservoir of the aggregates about to be captured. Thus aggregates that flow in the middle part of the reservoir can be captured by the colloidal deposit, in contrast to direct interception by the lateral walls. This also suggests that the probability to capture aggregates is increased when the surface of the pore becomes crowded.

In the following, we focus on the influence that the geometrical features and shape of the aggregates has on their capture. It turns out that aggregates that deposit in the pore have no preferential shape whatever their size. Actually, the distribution of the shape of the captured aggregates during clogging experiments is identical to that obtained from the stop and go experiment, simply meaning that it is a matter of probability (Fig. S4, ESI†). Nevertheless, we can go a bit further on the influence of the aggregate shape by considering that the probability of capturing aggregates is related to their maximum length or major axis, called here L_{max}, since the two opposite edges along L_{max} are the closest points to the pore walls during the aggregate rotation. We found that the capture probability increases and scales with the third power of L_{max} (Fig. 7). This suggests that aggregates act as "effective spheres" with a diameter equal to their long axes L_{max} as they enter into the pore. In other words, aggregates spin around their center of mass in such a way that their two edges along their greater dimension describes the surface of a sphere of diameter L_{max}.

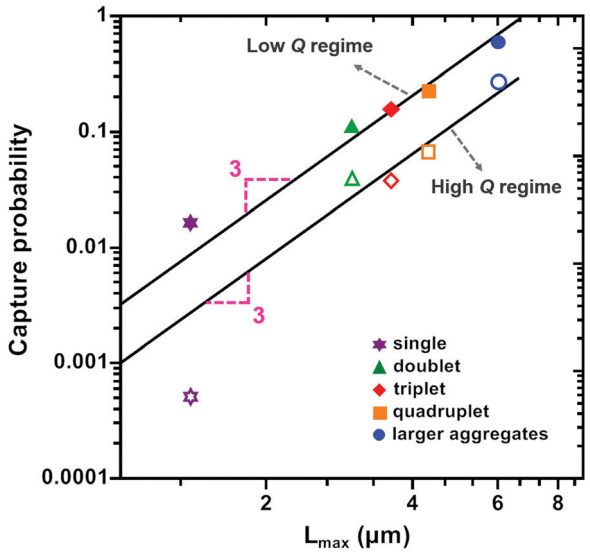

Fig. 7 Variation of the capture probability of aggregates with L_{max} for Q = 0.017 (top curve with full symbols) and 0.228 μL min^{-1} (bottom curve with empty symbols). The continuous lines are power law fits of the data with an exponent equal to 3. The value of L_{max} corresponds to the value of the median of the L_{max} distribution for the different aggregate sizes.

This evolution of the capture probability with diameter, L_{max}, is the same for both high and low flow regimes, but it appears to be greater in the low Q regime. We suppose that the higher rotation speed of the aggregates in this low flow regime[57] is responsible for such a behavior as this will mean that the edges of the aggregates will encounter the pore surface more frequently and thus increases their probability to be captured.

Summary and conclusions

In this paper we show that pores are mainly clogged by aggregates coming from the particle synthesis, when a predominantly monodisperse suspension of colloidal particles flows through a transparent model filter. In addition, we have determined the dynamics of aggregate particle deposition within a pore. Contrary to the work of Sauret *et al.*, the contaminant particles in our suspension are smaller than the pore size and thus pore clogging mainly results from the progressive accumulation of these aggregates and not from sieving a large aggregate. The analysis of the particle motion enables us to know what the shape and the size of the particles eventually captured are. We systematically found that aggregates, corresponding to a very small fraction of the suspension, *i.e.*, few percent, are actually responsible for the pore blocking. Unlike single particles, aggregates are able to deposit on the pore surface and on top of each other without being wiped off by the flow, since they can have multi contact points with the pore/colloidal deposit surface. The capture mechanism of aggregates is similar to that of single spherical particles, but in the former case there is physical interception of one of the two edges of the aggregates. As they flow through the channel, aggregates rotate around their center of mass, and thus behave as effective spheres with a diameter corresponding to their maximum length L_{max}, especially when they first enter in the constriction. Such a rotation enables the aggregates to get periodically closer to the pore or deposit surface and be captured, since the edges of the aggregates cannot always deviate from the deposit surface and avoid contact with it, unlike spherical particles that can more easily depart from the surface. The probability of aggregate capture is higher for low flow rates since the rotation speed of the aggregates is greater and thus increases their frequency of encountering the deposit/pore surface.[57]

We performed clogging experiments with other suspensions, which were stabilized only by charge on their surface (for instance sulfate groups), obtained from different companies and also observed systematically that pore blocking results from aggregate accumulation. In each case there are between 0.5 and 2% of aggregates in the suspensions, before they are injected in the microfluidic devices. The geometrical features of these aggregates also remain unchanged until they deposit in the pores, *i.e.*, they are not broken by the flow while they are transported through the microfluidic channel.

We think that pore clogging by aggregates will also be observed in two other common situations in which aggregates are formed inside the porous structure. In a first situation, flow can induce particle aggregation in the bulk of the flowing suspension and also breaks up the aggregates. In a second one, colloidal particles can form a deposit on the pore walls but its growth can be limited by the flow that erodes its surface, releasing aggregates that may be captured further downstream. Generally speaking, this experimental work clearly shows that in order to draw sound conclusions on the dynamics of clog formation one must have to (i) know precisely the distribution of size and shape of the particles/aggregates that compose the suspension about to be filtered and (ii) be able to capture the dynamics of particle deposition in the pore. This methodology has to be used with different colloidal suspensions to check whether or not aggregates are indeed the main objects that accumulate and eventually block the pores.

Conflicts of interest

There are no conflicts of interest to declare.

References

1 D. C. Mays and J. R. Hunt, *Environ. Sci. Technol.*, 2005, **39**, 577–584.
2 R. Gopal, S. Kaur, Z. Ma, C. Chan, S. Ramakrishna and T. Matsuura, *J. Membr. Sci.*, 2006, **281**, 581–586.
3 L. Sicignano, G. Tomaiuolo, A. Perazzo, S. P. Nolan, P. L. Maffettone and S. Guido, *Chem. Eng. J.*, 2018, **341**, 639–647.
4 E. Dressaire and A. Sauret, *Soft Matter*, 2017, **13**, 37–48.
5 Q. Liu, B. Zhao and J. C. Santamarina, *J. Geophys. Res.: Solid Earth*, 2019, **124**, 9495–9504.

6 Y. Chen, J. C. Sabio and R. L. Hartman, *J. Flow Chem.*, 2015, **5**, 166–171.
7 A. Sauret, E. C. Barney, A. Perro, E. Villermaux, H. A. Stone and E. Dressaire, *Appl. Phys. Lett.*, 2014, **105**, 074101.
8 A. Sauret, K. Somszor, E. Villermaux and E. Dressaire, *Phys. Rev. Fluids*, 2018, **3**, 104301.
9 V. Ramachandran and H. S. Fogler, *J. Fluid Mech.*, 1999, **385**, 129–156.
10 V. Ramachandran and H. S. Fogler, *Langmuir*, 1998, **14**, 4435–4444.
11 G. C. Agbangla, E. Climent and P. Bacchin, *Comput. Fluids*, 2014, **94**, 69–83.
12 H. M. Wyss, D. L. Blair, J. F. Morris, H. A. Stone and D. A. Weitz, *Phys. Rev. E: Stat., Nonlinear, Soft Matter Phys.*, 2006, **74**, 061402.
13 B. Dersoir, M. Robert de Saint Vincent, M. Abkarian and H. Tabuteau, *Microfluid. Nanofluid.*, 2015, **19**, 953–961.
14 B. Dersoir, A. B. Schofield and H. Tabuteau, *Soft Matter*, 2017, **13**, 2054–2066.
15 B. Dersoir, A. B. Schofield, M. Robert de Saint Vincent and H. Tabuteau, *J. Membr. Sci.*, 2019, **573**, 411–424.
16 T. van de Laar, S. ten Klooster, K. Schroën and J. Sprakel, *Sci. Rep.*, 2016, **6**, 28450.
17 D. C. Duffy, J. C. McDonald, O. J. A. Schueller and G. M. Whitesides, *Anal. Chem.*, 1998, **70**, 4974–4984.
18 A. Accardo, R. Courson, R. Riesco, V. Raimbault and L. Malaquin, *Addit. Manuf.*, 2018, **22**, 440–446.
19 C. M. Cejas, F. Monti, M. Truchet, J.-P. Burnouf and P. Tabeling, *Langmuir*, 2017, **33**, 6471–6480.
20 B. Mustin and B. Stoeber, *Langmuir*, 2016, **32**, 88–101.
21 P. Bacchin, A. Marty, P. Duru, M. Meireles and P. Aimar, *Adv. Colloid Interface Sci.*, 2011, **164**, 2–11.
22 Z. B. Sendekie, A. Gaveau, R. G. Lammertink and P. Bacchin, *Sci. Rep.*, 2016, **6**, 31471.
23 S. S. Massenburg, E. Amstad and D. A. Weitz, *Microfluid. Nanofluid.*, 2016, **20**, 94.
24 Z. B. Sendekie and P. Bacchin, *Langmuir*, 2016, **32**, 1478–1488.
25 T. van de Laar, S. ten Klooster, K. Schroën and J. Sprakel, *Sci. Rep.*, 2016, **6**, 28450.
26 R. van Zwieten, T. van de Laar, J. Sprakel and K. Schroën, *Sci. Rep.*, 2018, **8**, 5687.
27 B. Mustin and B. Stoeber, *Microfluid. Nanofluid.*, 2010, **9**, 905–913.
28 J. Linkhorst, T. Beckmann, D. Go, A. J. C. Kuehne and M. Wessling, *Sci. Rep.*, 2016, **6**, 22376.
29 J. Linkhorst, J. Rabe, L. T. Hirschwald, A. J. C. Kuehne and M. Wessling, *Sci. Rep.*, 2019, **9**, 18998.
30 I. Bouhid de Aguiar, M. Meireles, A. Bouchoux and K. Schroën, *Sci. Rep.*, 2019, **9**, 9241.
31 J. Lohaus, F. Stockmeier, P. Surray, J. Lölsberg and M. Wessling, *J. Membr. Sci.*, 2020, **602**, 117886.
32 G. Brans, A. van Dinther, B. Odum, C. G. P. H. Schroën and R. M. Boom, *J. Membr. Sci.*, 2007, **290**, 230–240.
33 M. E. Warkiani, F. Wicaksana, A. G. Fane and H.-Q. Gong, *Microfluid. Nanofluid.*, 2015, **19**, 307–315.
34 I. S. Ngene, R. G. H. Lammertink, M. Wessling and W. van der Meer, *J. Membr. Sci.*, 2010, **346**, 202–207.
35 I. S. Ngene, R. G. H. Lammertink, M. Wessling and W. G. J. Van der Meer, *J. Membr. Sci.*, 2011, **368**, 110–115.
36 A. Marin, H. Lhuissier, M. Rossi and C. J. Kähler, *Phys. Rev. E*, 2018, **97**, 021102.
37 M. Souzy, I. Zuriguel and A. Marin, *Phys. Rev. E*, 2020, **101**, 060901.
38 G. Gerber, M. Bensouda, D. A. Weitz and P. Coussot, *Phys. Rev. Lett.*, 2019, **123**, 158005.
39 C. Duchêne, V. Filipe, S. Huille and A. Lindner, *Soft Matter*, 2020, **16**, 921–928.
40 P. Bacchin, P. Aimar and V. Sanchez, *J. Membr. Sci.*, 1996, **115**, 49–63.
41 S. Bounoua, S. Tomas, J. Labille, B. Molle, J. Granier, P. Haldenwang and S. N. Izzati, *Irrig. Sci.*, 2016, **34**, 327–342.
42 R. Guha, X. Shang, A. L. Zydney, D. Velegol and M. Kumar, *J. Membr. Sci.*, 2015, **479**, 67–76.
43 A. Bretagne, F. Cotot, M. Arnaud-Roux, M. Sztucki, B. Cabane and J.-B. Galey, *Soft Matter*, 2017, **13**, 3812–3821.
44 S. Shin, J. T. Ault, P. B. Warren and H. A. Stone, *Phys. Rev. X*, 2017, **7**, 041038.
45 M. Emmanuel, D. Horváth and Á. Tóth, *CrystEngComm*, 2020, **22**, 4887–4893.
46 G. Laffite, C. Leroy, C. Bonhomme, L. Bonhomme-Coury, E. Letavernier, M. Daudon, V. Frochot, J. P. Haymann, S. Rouzière, I. T. Lucas, D. Bazin, F. Babonneau and A. Abou-Hassan, *Lab Chip*, 2016, **16**, 1157–1160.
47 R. L. Hartman, J. R. Naber, N. Zaborenko, S. L. Buchwald and K. F. Jensen, *Org. Process Res. Dev.*, 2010, **14**, 1347–1357.
48 R. L. Hartman, *Org. Process Res. Dev.*, 2012, **16**, 870–887.
49 A. Perazzo, L. Sicignano, G. Tomaiuolo, R. Marotta, R. Andreozzi and S. Guido, *Chem. Eng. Sci.*, 2019, **207**, 581–587.
50 M. Trofa, G. D'Avino, L. Sicignano, G. Tomaiuolo, F. Greco, P. L. Maffettone and S. Guido, *Chem. Eng. J.*, 2019, **358**, 91–100.
51 T. M. Squires and S. R. Quake, *Rev. Mod. Phys.*, 2005, **77**, 977.
52 S. Shen, E. D. Sudol and M. S. El-Aasser, *J. Polym. Sci., Part A: Polym. Chem.*, 1993, **31**, 1393–1402.
53 Y. Almog, S. Reich and M. Levy, *Br. Polym. J.*, 1982, **14**(4), 131–136.
54 G. Loy and A. Zelinsky, *IEEE Trans. Pattern Anal. Mach. Intell.*, 2003, **25**, 959–973.
55 S. Veerapaneni and M. R. Wiesner, *J. Colloid Interface Sci.*, 1996, **177**, 45–57.
56 L. A. Spielman, *Annu. Rev. Fluid Mech.*, 1977, **9**, 297–319.
57 K. Li and H. Ma, *Langmuir*, 2018, **34**, 2967–2980.
58 M. B. Salerno, M. Flamm, B. E. Logan and D. Velegol, *Environ. Sci. Technol.*, 2006, **40**, 6336–6340.